Efficient Optimization of Airbags by the Measurement of the Time Resolved Strain Distribution on Airbag Covers

Ralf Lichtenberger, Hubert Schreier

LIMESS Messtechnik u. Software GmbH, D-75180 Pforzheim

1 Introduction

The demand for accurate, time-resolved full-field deformation measurements has led to the development of new techniques for optical deformation measurement technology. These techniques are ideally suited for FEM model verification, for the determination of material characteristics under quasi-static or dynamic loading conditions and for component testing. In this article we introduce a measurement technology based on digital image correlation which is applicable to three-dimensional measurement problems. With the use of latest high speed cameras, measurements of the displacement distribution and the strain distribution on airbag covers during the deployment can be accomplished. This data is used to optimize the deformation and opening behaviour of the covers reducing therefore the injury risk of the passenger and the costs of development and manufacturing of airbag modules. The results can be compared to FEM simulations and the underlying mechanical models can be further improved. These cost-effective optimizations are becoming more and more important as new materials and joining methods are being introduced into the automotive manufacturing industry.

2 Digital Image Correlation

The digital image correlation technique was originally introduced in the early '80s by researchers from the University of South Carolina [1]. The idea behind the method is to infer the displacement of the material under test by tracking the deformation of a random speckle pattern in digital images acquired during the loading (Figure 1). The image analysis process can be understood as a pattern recognition technique,

that searches locally the random speckle pattern by comparing the images of the deformed with the reference state. With a single camera, the in-plane displacement components *u, v* and the strain components *exx, eyy, exy, e1, e2* can be measured on a flat specimen.
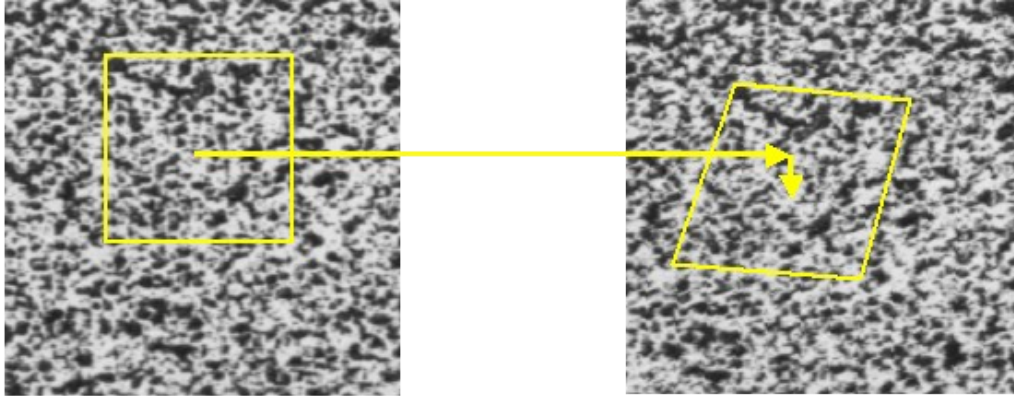

Figure 1: Undeformed and deformed image with subset. The mapping function permits the matching of square areas from the undeformed image to non-square areas in the deformed image.

More recently, the DIC method has been extended to use multiple cameras, permitting the measurement of three-dimensional shape as well as the measurement of the three-dimensional deformation [2]. The three-dimensional technique requires the use of at least two synchronized cameras acquiring images of the loaded specimen from different viewing angles. By determining corresponding image locations across views from the different cameras and tracking the movement throughout the loading cycle, the shape and deformation can be reconstructed based on a simple camera calibration. Using two or more cameras the objects coordinates *x,y,z* the displacements *u,v,w* and the strain components in the surface are measured. Rigid body movements are taken into account.

2.1 Measurement Setup

The experimental setup for the 3D DIC method is comparatively simple and illustrated in Figure 2. The two cameras are mounted on a rigid bar to avoid relative motion of the cameras.
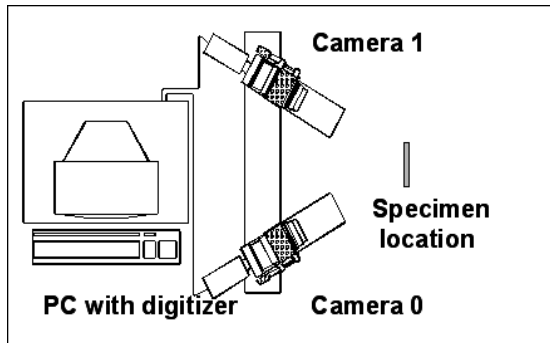
Figure 2: Stereoscopic setup for 3D-deformation measurement.

The DIC method does not require the use of lasers and the specimen can be illuminated by means of a white-light source. However, the specimen surface must have a fairly uniform random pattern, which is typically applied to the specimen before the test. Among the many methods for pattern application are self-adhesive, pre-printed patterns, stamps and application of paint speckles with air-brushes, spray cans or brushes.

2.2 Image Analysis

Though a large variety of DIC algorithms have been developed over the years [1,3,4,5,6], one particular method has established itself as the preferred method for deformation analysis due to it's capability to measure arbitrarily large rotations and strains in excess of 500%, as well as it's superior accuracy and efficient implementation. As the deformed coordinates will not fall onto the sampling grid of the image, accurate grey-value interpolation techniques are required to achieve optimal sub-pixel accuracy without bias [4].

For three-dimensional shape measurements, a similar algorithm is used. However, the mapping function is now based on the known calibration parameters of the cameras, and the sought parameters are the location and orientation of a segment of the surface assumed to be locally planar. For deformation measurements, additional parameters describing the orientation and position of the surface segment after deformation as well as parameters describing higher-order deformation terms are added to the mapping functions. This process can be interpreted as a projection/back projection approach, as illustrated in Figure 3.
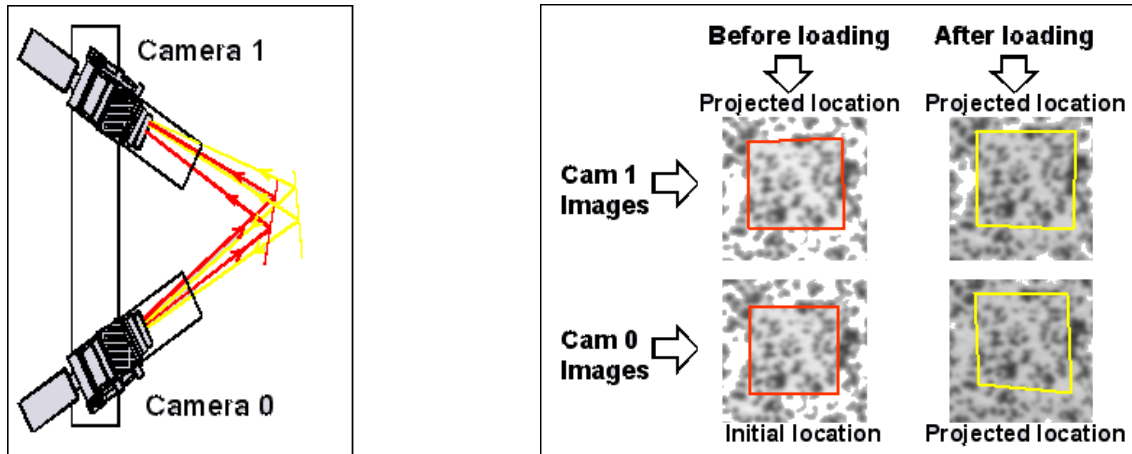
Figure 3: 3D measurement principle. Usage of projection and back projection method to determine the position and displacement of small segments of the surface.

2.3 Calibration

As opposed to two-dimensional systems, where camera calibration is simply the determination of a scale factor, three-dimensional systems have to be calibrated. Commonly, a pin-hole camera model with Seidel lens distortions is used. The automatic calibration process involves the acquisition of a series of images of a calibration target in different orientations (rotations around all three axes). Two example images are shown in Figure 4. From the images of the calibration target, inner parameters for the two cameras as well as their relative orientation can be determined fully-automatically [8] within seconds. Once the system is calibrated, images of the specimen undergoing deformation are acquired.
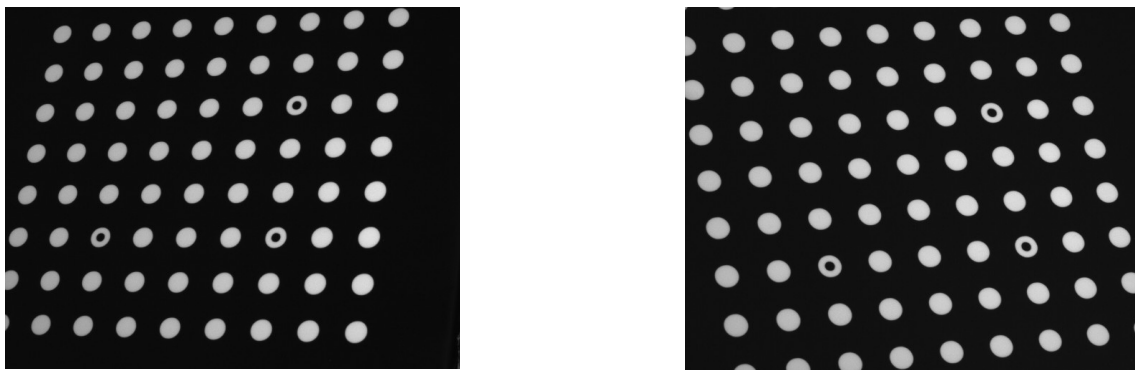

Figure 4: Example images of the calibration grid taken from left and right camera.

For a 3D deformation measurement multiple correlations are performed between the images:

1. Stereo matching between left and right camera to calculate the 3D coordinates (shape) of the specimen.

2. Temporal tracking between deformed images and reference images to calculate the displacement and deformation of the specimen.

Figure 5 illustrates the multiple correlations between the images. From the correlation the measurement accuracy is calculated and gives a measurement quality feedback.
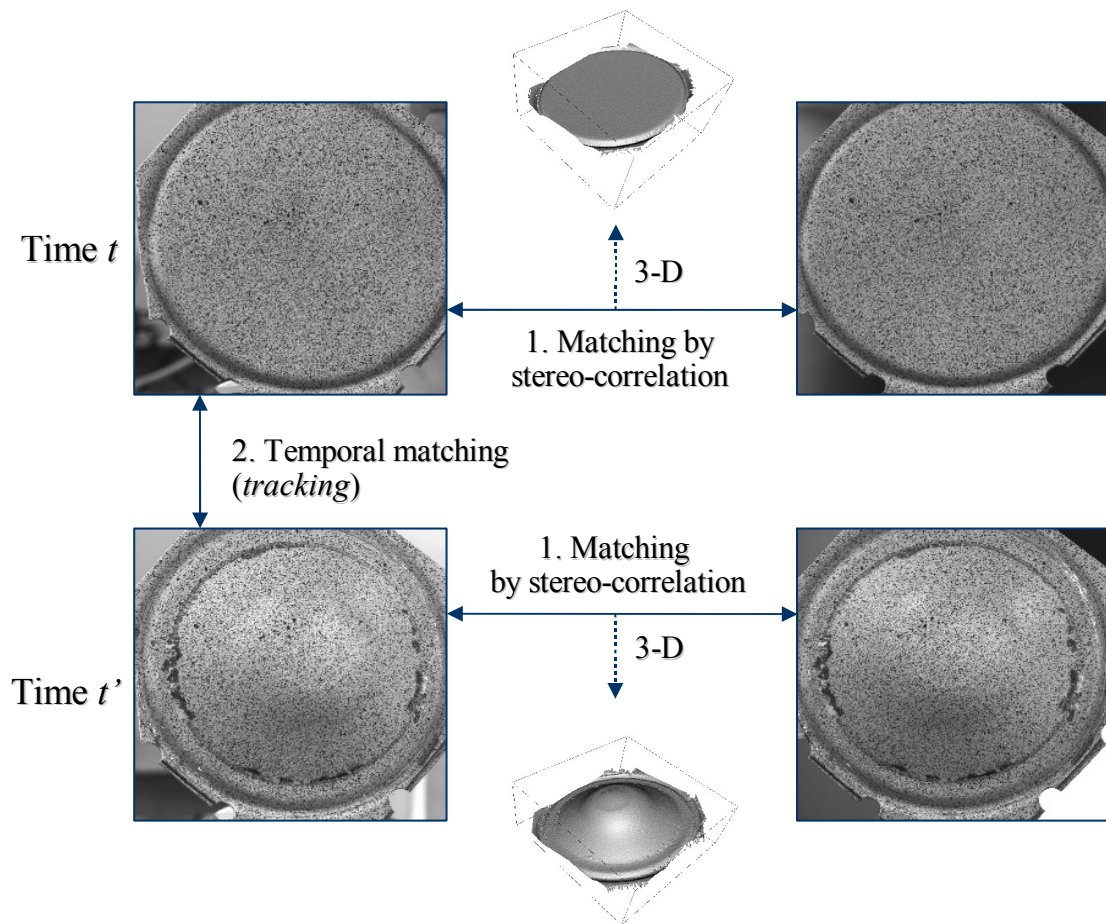

Figure 5: Multiple correlations for a 3D deformation measurement.

3 Example

This example describes the measurement of a passenger airbag module by the usage of two synchronized high speed colour cameras with a resolution of 512x384 pixel at a speed of 2000fps. The measurement was performed until a crack occurs at the hyphenation point (third image at t=1.5ms). The measurement accuracy and resolution could be improved by using b/w cameras without Bayer pattern and by more recent cameras with higher resolution and recoding rate.

Figure 6 shows the left and right camera images, that are recorded simultaneously from different view points. The left image shows the u-shaped hyphenation point as black line. The dark grey area in the left camera image is the selected analysis area in which the image correlation is performed. A coordinate transformation sets the directions of the coordinate axis according to the white marker in figure 6 left.
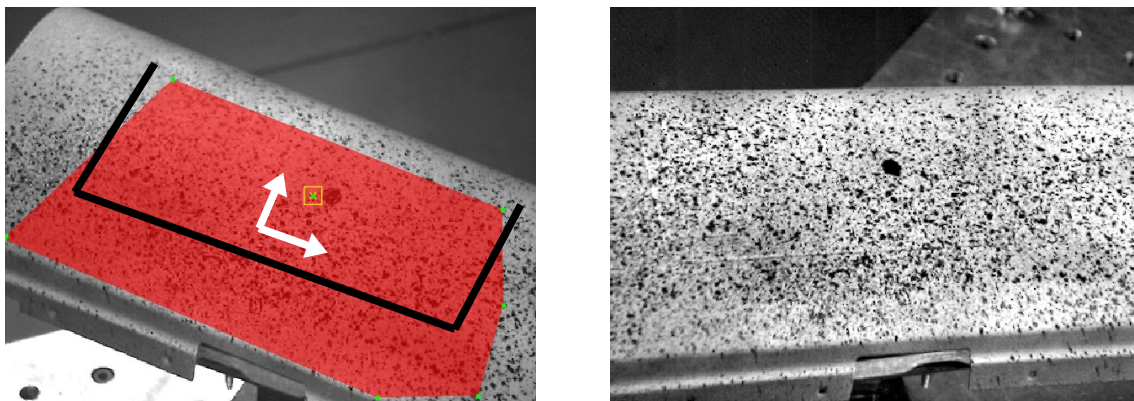

Figure 6: Left and right speckle pattern image of the airbag cover. The left image shows the analysed region (red AOI), the hyphenation point (black line) and the coordinate system (white). The z-axis points towards the passenger.

From each image set (left and right camera) the surface's 3D coordinates at every image point (pixel), resp. the object's shape is measured. Figure 7 shows the 3D visualization of the airbag cover's shape. The mapped grey colour represents the *z*-coordinate.
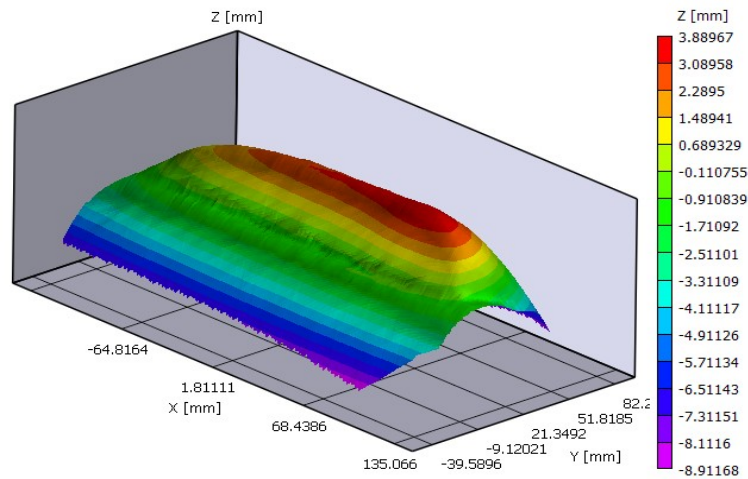
Figure 7: 3D view of the measured shape (deformed image 1ms). The mapped grey colour represents the z-value of the object coordinates.

From the temporal matching of the pattern the 3D displacements ($u,v,w,$) are calculated. This can be visualized in different ways. Figure 8 shows the 3D shape from the right viewing direction (along the x-axis) for three deformed states. The grey colour represents the w component scaled from 0.0 to 7.6mm.
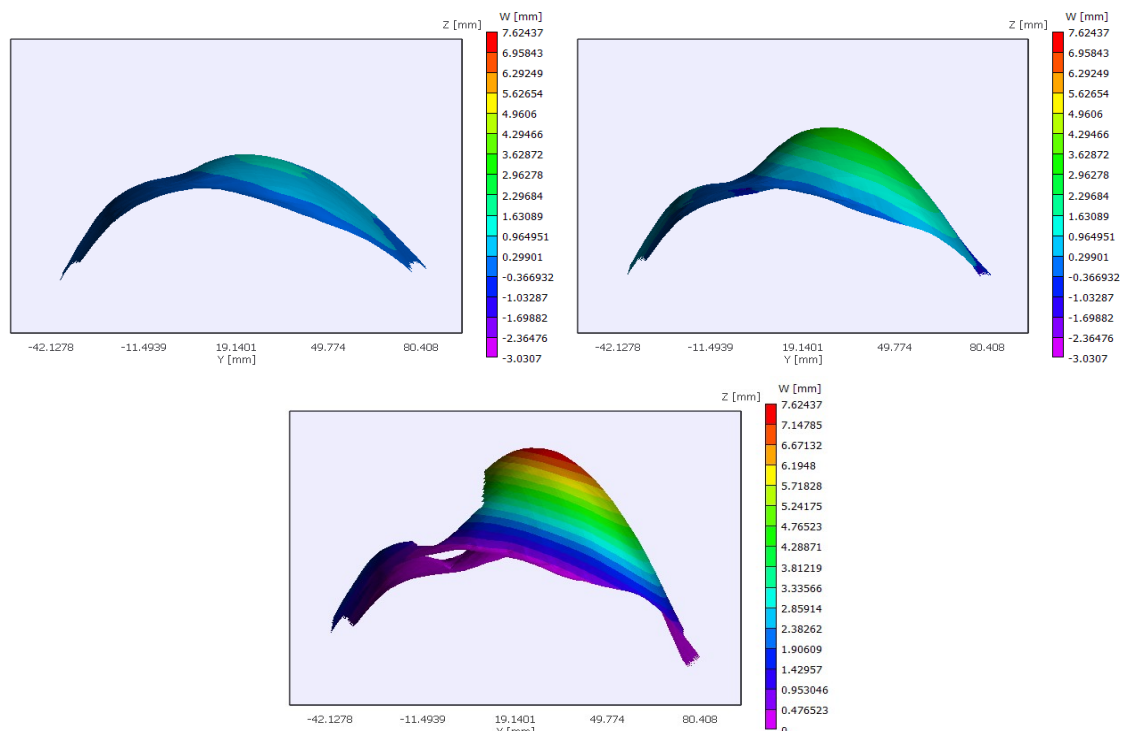

Figure 8: Right view (along x-axis) of the measured airbag cover shape for the times 0.5ms, 1.0ms and 1.5ms. The scaling is fixed for all images.

From the displacements the local velocities and accelerations of all displacement and strain components can be be calculated.

Figure 9 shows the *w*-displacement component as grey colour map on the left camera image. The results show that the load from the airbag/gas generator is not induced symmetrically. For all deformed states the *w*-displacement are larger at the right side of the module.
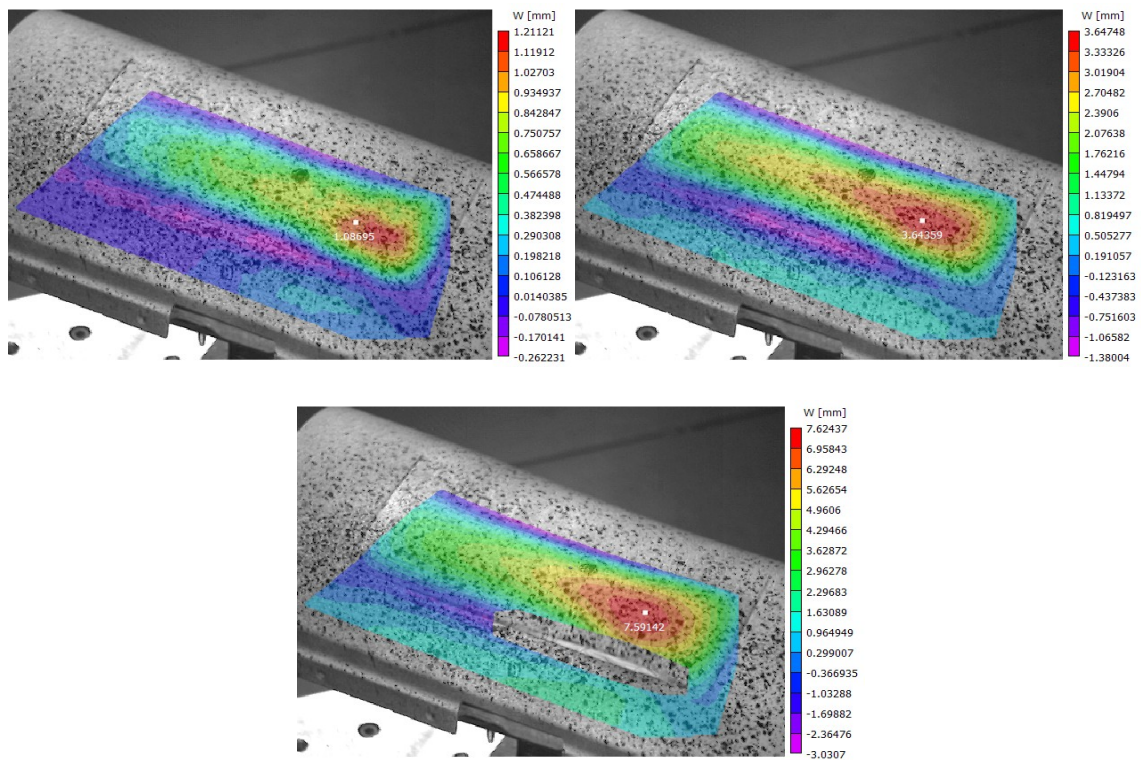

Figure 9: Grey colour overlay of the measured displacement component w (out-of-plane-direction) for the deformed states at t=0.5ms, 1.0ms and 1.5ms.

The strain in the object's surface is calculated from the displacements according to the Lagrangian approach. Figure 10 shows the strain distribution mapped as grey colour on the left camera image. The strain component *Exx* has a maximum (white) at the right hyphenation line reflecting the inhomogenous pressure. The strain component *Eyy* has a strong minimum (black) along the hyphenation point line.
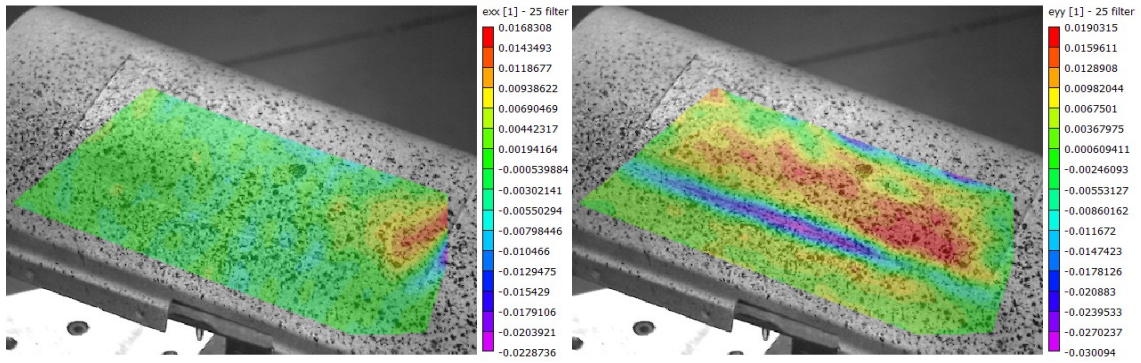
Figure 10: Grey coded overlay of the measured strain components *Exx* (parallel to hyphenation point) and *Eyy* (vertical to hyphenation point) for the state at 1.0ms.

The measured displacements and strains are extracted along a vertical and a horizontal line for different times. Figure 11 shows these lines in the y-coordinate map image.
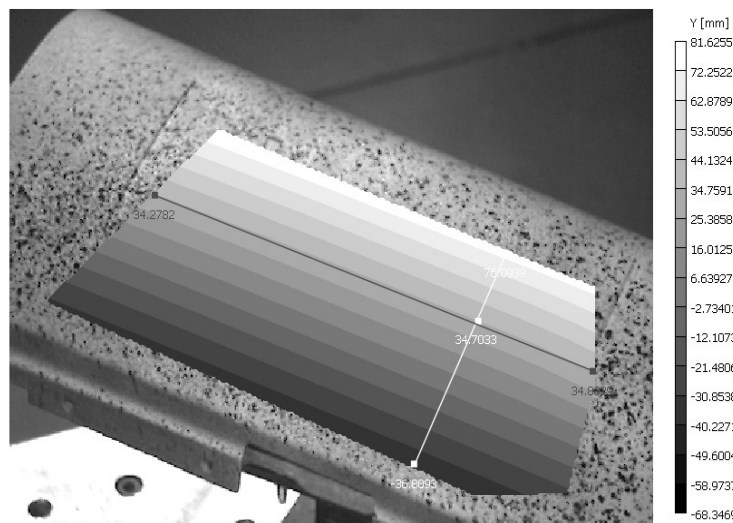

Figure 11: Mapped y-coordinate with data extraction lines in *x*-direction (black) and *y*-direction (white).

In the diagrams of figure 12 the *w*-displacement is plotted against the extracted line coordinates. The left diagram shows an increasing *w*-displacement from left to right. This reflects the non-uniform pressure from airbag and gas generator.

The right diagram in figure 12 show the w-displacement along the line in *y*-direction. (For t=1.5ms the curve contains no data around the crack.)
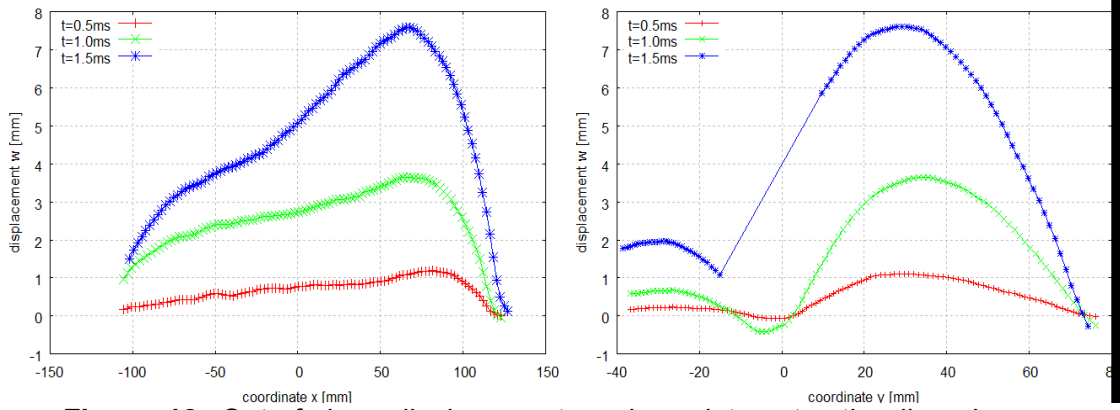
Figure 12: Out-of-plane displacement *w* along data extraction lines in x- and y direction.

Figure 13 shows the strain Eyy for the two line extractions. The strain *Eyy* in the airbag cover's surface is increasing with time and slightly higher on the right side of the cover. The data extraction along the *y*-direction is shown in the right diagram if figure 13. Before the crack occurs the strain *Eyy* is negative (compression) at the hyphenation line around *y*=0.0mm.
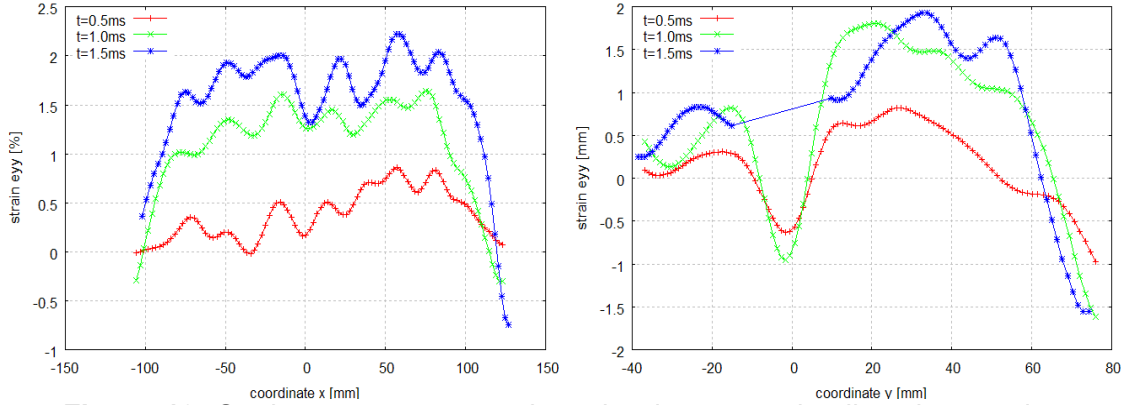

Figure 13: Strain component eyy along the data extraction lines in x- and y direction.

It is important that a hyphenation point is loaded with tension, because it may not open properly under compressive loads. From the right diagram in figure 12 it can be seen that the hyphenation point has smaller *w*-displacements than the surrounding. It therefore acts like a hinge, resulting in compression on the surface and tension on the underside. A tensile loading of the hyphenation point can be achieved by modifying the airbag folding and gas generator such that the *w*-displacement at the hyphenation point is increased.

4 Summary and Conclusion

In this paper, we have given a brief overview of an accurate technology to measure non-contact and full-field displacement, deformations and strains. The simple and robust setup is well-suited to both laboratory and field conditions and minimal specimen preparation is required. In combination with high speed cameras this technology can be easily used for highly dynamic impact, crash and component testing.

The measurement results of the cover during the first milliseconds of an airbag's deployment show unexpected strain distributions around the hyphenation point. This could cause, that parts are catapulted away with high velocity if the cover breaks in a location other than the hyphenation point. It is clear that this measured airbag module must be further optimized for passenger safety.

Due to the meaningful and accurate results the application field of the digital image correlation technique is very large and leads to cost reduction in system development and manufacturing.

The key points of the technology and analysis software are:
- Curved or planar objects from 10x10mm to more than 10x10m size
- Accuracy unaffected by large in-plane rotations or translations
- Accuracy up to +/-0.01 pixels in displacement (e.g. 0.01mm at 1x1m measurement field with mega pixel camera)
- Accuracy > 200 microstrain
- Strain levels in excess of 100% have been successfully measured
- Complex loading (combined tension/torsion, compression, pressurization etc.)
- Quasi-static to ultra-high speed events.

5 References

1. Peters, W.H. and Ransom, W.F., *Digital imaging techniques in experimental stress analysis*, Opt. Eng., 21(3), pp. 427-431, 1892

2. Helm, J.D., McNeill, S.R. and Sutton, M.A., *Improved 3-D image correlation for surface displacement measurement,* Opt. Eng., 35(7), pp. 1911-1920, 1996

3. Sutton, M.A., Cheng, M., Peters, W.H., Chao, Y.J. and McNeill, S.R., *Application of an optimized digital correlation method to planar deformation analysis*, Image and Vision Computing, 4(3), pp. 143-151, 1986

4. Schreier, H.W., Braasch, J.R. and Sutton, M.A., *Systematic Errors in digital image correlation caused by gray-value interpolation*, Opt. Eng., 39(11), pp. 2915-2921, 2000

5. Chen, D.J., Chiang, F.P., Tan, Y.S. and Don, H.S., *Digital speckle displacement measurement using a complex fourier spectrum method,* Applied Optics, 32(11), pp. 1839-1849, 1993

6. Synnergren, P. and Sjoedahl, M., *A stereoscopic digital speckle photography system for 3-d displacement field measurements*, Optics and Lasers in Engineering, 31, pp. 425-433, 1999

7. Vic-2D Digital Image Correlation Software, Correlated Solutions, Inc., www.correlatedsolutions.com

8. Triggs, B., McLauchlan, P., Hartley, R. and Fitzgibbon, A. *Bundle adjustment - a modern synthesis,* Vision Algorithms: Theory and Practice, Springer Verlag, 2000

9. Vic-3D Digital Image Correlation Software, Correlated Solutions, Inc., www.correlatedsolutions.com